Xiongfei Lv[1]
Department of Astronautic Science and Mechanics,
Harbin Institute of Technology (HIT),
No. 92 West Dazhi Street,
P.O. Box 301,
Harbin 150001, China

Liwu Liu[1]
Department of Astronautic Science and Mechanics,
Harbin Institute of Technology (HIT),
No. 92 West Dazhi Street
P.O. Box 301,
Harbin 150001, China

Yanju Liu[2]
Department of Astronautic Science and Mechanics,
Harbin Institute of Technology (HIT),
No. 92 West Dazhi Street,
P.O. Box 301,
Harbin 150001, China
e-mail: yj_liu@hit.edu.cn

Jinsong Leng[2]
Centre for Composite Materials and Structures,
Harbin Institute of Technology (HIT),
No. 2 Yikuang Street,
P.O. Box 3011,
Harbin 150080, China

Electromechanical Modeling of Softening Behavior for Dielectric Elastomers

Dielectric elastomer (DE) is a promising electroactive polymer. As DE material, rubbers are often filled with functional particles to improve their electromechanical performance. However, the filled particles also bring stress softening, which is known as Mullins effect. In this paper, we prepared the carbon nanotube filled silicone elastomer (SE) as DE composite and modeled its Mullins effect using the pseudo-elastic theory. Then, the thermodynamics of DE was combined to predict the idealized electromechanical softening behavior. Two cases are considered: linear dielectric and saturated dielectric. For linear dielectric with an initial force, "residual strain" will appear after every voltage-controlled cycle, and instability may be eliminated in reloading. For saturated dielectric, the material response changes a lot after saturation, which also affects the subsequent softening behavior. At last, viscoelasticity was further incorporated to account for rate-dependent softening deformation, and we also carried out some simple electromechanical experiments on VHB 4910 to explore its softening behavior. This work may lead to a better understanding of the softening behavior in DEs undergoing electromechanical coupling situations. [DOI: 10.1115/1.4040405]

Keywords: dielectric elastomer composite, Mullins effect, softening behavior, electromechanical coupling, viscoelasticity

1 Introduction

Dielectric elastomer (DE) is a kind of soft and insulating materials. When a DE membrane sandwiched between two compliant electrodes is subject to a high voltage, due to its high dielectric constant and low modulus, Maxwell stress will cause the membrane to reduce thickness and expand area. This electromechanical transduction and its inverse process enable the mutual conversion between mechanical and electrical energy. Besides, the materials also possess desirable attributes, including good biological compatibility, high energy density, fast response, light weight, low price, easy processing and manufacturing, etc [1–3]. Therefore, dielectric elastomers are now widely recognized as a kind of high-tech smart material, which has a variety of applications, ranging from bionic robots to energy harvesting [4–7].

As a sort of DE material, rubbers are usually restricted by their electromechanical coupling performance. One solution is to enhance their dielectric property by filling functional particles [3,8,9]. However, from the perspective of mechanics, the influence brought by filled particles has not been clearly recognized. Rubber is a three-dimensional network composed of coiled molecular chains, which have different lengths, and is held together by crosslinks. By filling additional particles, these molecular chains are adsorbed on the particle surfaces [10,11]. When the rubber is subject to loads, the chains will slip and slide with friction on these particles [10,11], which may result in the chain length increase between two particles after unloading (as chain AA′ in Fig. 1). Subject to loads again, the slipping and sliding are mostly eliminated until the deformation reaches the former level; therefore, the required loads decrease. The stress softening under cyclic load is a typical trait of filled rubbers, which is widely known as Mullins effect [12,13]. Besides the filled rubbers, stress softening is also reported in the most commonly used commercial dielectric elastomer material, VHB 4910/4905 tapes [14].

The idealized macro performance of Mullins effect is shown in Fig. 2. When we monotonously stretch the material, the loading path goes along $P_0AP_1BP_2$. If we unload it at point P_1, the unloading path will be below the loading path, such as $P_1A'P_0$, and the subsequent reloading path will follow the unloading path before exceeding the previous unloading point P_1. After that, it will recover the monotonous loading path P_1BP_2.

Stress softening affects the mechanical performance of dielectric elastomers. In general, in order to obtain the real and stable mechanical performance, the dielectric elastomers must be pre-stretched several cycles to eliminate stress softening before

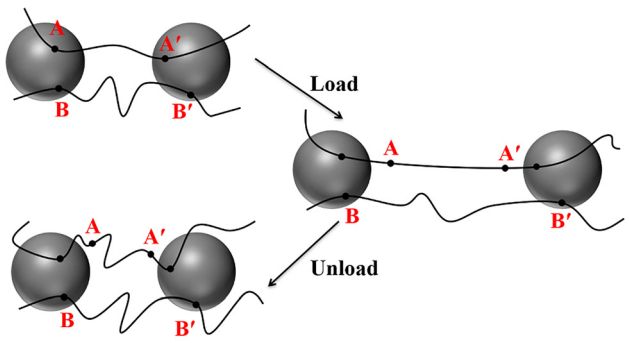

Fig. 1 Molecular chains and particles before, during, and after loading

[1]X. Lv and L. Liu contributed equally to this work.
[2]Corresponding authors.

Contributed by the Applied Mechanics Division of ASME for publication in the Journal of Applied Mechanics. Manuscript received January 30, 2018; final manuscript received May 20, 2018; published online August 31, 2018. Assoc. Editor: Junlan Wang.

testing. However, in practical applications, the effect cannot be neglected and we should design the applications (such as actuators, soft robots, and flapping wings) in terms of the real and stable mechanical performance after softening. Therefore, we need to know the softening behavior, and the related study is necessary.

To model the effect, Mullins and Tobin [15] assumed that the filled rubber exists in two phases, the hard and soft phases. They considered that the material is full of hard phases at the beginning, as the deformation increases, some hard phases gradually fracture into soft phases so that the material softens. Thereafter, many researchers have modeled Mullins effect. Ogden and Roxburgh [16] developed a pseudo-elastic theory to consider the Mullins effect. In this theory, they used an error function to modify the strain energy function to change the stress during the unloading and reloading process. Based on this method, some researchers have tried to make the model more applicable in a wide scope. Dorfmann and Ogden [17] replaced the error function by a hyperbolic tangent function. Soon afterward, they [18] also extended their model to consider both the stress softening and the residual strain. Yeom et al. [19] modified Dorfmann and Ogden model [17] by introducing a nonlinear factor to describe high nonlinearity. Rickaby and Scott [20–22] comprehensively combined the inelastic features of stress relaxation, hysteresis, and residual strain together to develop a model, which is able to describe the Mullins effect for both stretch and compression. However, dielectric elastomer needs to operate under electromechanical coupling field. Similarly, softening will also happen. To the authors' knowledge, the related research is barely reported. Accordingly, we are going to study the electromechanical softening behavior in this paper.

This paper is organized as follows: The preparation of carbon nanotube (CNT) filled silicon elastomer and softening test are presented in Sec. 2. Section 3 demonstrates the application of the pseudo-elastic theory on our material. Then, considering linear dielectric and saturated dielectric, we theoretically analyzed of the idealized softening behavior under electromechanical coupling field in Sec. 4. We further introduced the viscoelastic model and carried out experiments on VHB 4910 to explore its electrometrical softening behavior in Sec. 5. At last, all results are summarized in Sec. 6.

2 Preparation and Testing of Carbon Nanotube Filled Silicon Elastomers

The CNT filled silicone elastomer (SE) was prepared as the dielectric elastomer composite (DEC). The silicone elastomer is TC 5005 A/B-C produced by BJB Enterprises, Inc., Tustin, CA. It is a room temperature curing polydimethyl siloxane with three components. Component A is silicone rubber base; component B is catalyst; and component C is silicone fluid. TC-5005 A/B is processed by adding curing agent B at a ratio of 10 parts by weight to 100 parts by weight of A. Component C can be as much as 50% to the total weight of TC-5005 A/B. Multiwalled carbon nanotubes with length 30 μm and outer diameter 20–30 nm were used. Figure 3 shows the preparation process of the dielectric elastomer composite. Component C with 20% weight ratio was added to synthesis the silicone matrix. The CNTs were first dried in vacuum oven at 200 °C for 24 h to eliminate trapped air bubble and moisture. At last, the processed CNTs were mixed in silicone matrix and stirred using centrifugal blender; then the mixture was poured into a mold and cured under room temperature.

In our pervious study, we have explored the amount of filling and the resulting enhancement of its dielectric properties of the composites with respect to that of the pure silicone [9]. Figure 4 presents room-temperature dielectric spectra for both the pure silicone and the composites (CNT weight percentage of 1, 2, 3, 4, and 5) in the range of 10e2–10e7 Hz. Both the relative permittivity and dielectric loss spectra monotonically decrease with frequency over the whole range. As expected, by increasing the carbon nanotube content, a progressive increase of permittivity of the composites is achieved at all frequencies compared to pure silicone. That is to say the permittivity of dielectric elastomer composites could be significantly improved by adding CNT particles.

To reflect the influence of particle content, the composites with particle weight percentage of 3 and 5 (named 3% CNT/SE and 5% CNT/SE for short in the rest of paper, respectively) were tested by a stepwise cyclic tensile test to characterize the Mullins effect. Rectangle specimens with the dimension 100 mm × 25 mm × H (0.89 mm for 3% CNT/SE and 0.80 mm for 5% CNT/SE) were cut out from the membrane. The test was conducted on Zwick/Roell Z010 universal testing machine with an optic extensometer. The loading rate was 200 mm/min, and the step strain and maximal strain was 50% and 250%. Before the test, a preload of approximately 0.1 N was induced to eliminate out-of-plane buckle introduced during the clamping process.

The step-up curves in Figs. 5(*a*) and 5(*c*) show obvious stress softening. The loading and unloading curves of 3% CNT/SE basically coincide within the first two cycles, showing nearly no Mullins effect, and the stress starts to soften from the third cycle, while the 5% CNT/SE shows great stress softening since the first cycle. That is to say, the higher filler content performs greater stress softening. Besides, we also observe obvious and increasing residual strain, which increases with the amount of filler content and the amplitude of stretch. In the step-down test, Fig. 5(*b*) presents that the following unloading and reloading curves coincide with the first unloading curve, which also demonstrates the internal mechanism of Mullins effect.

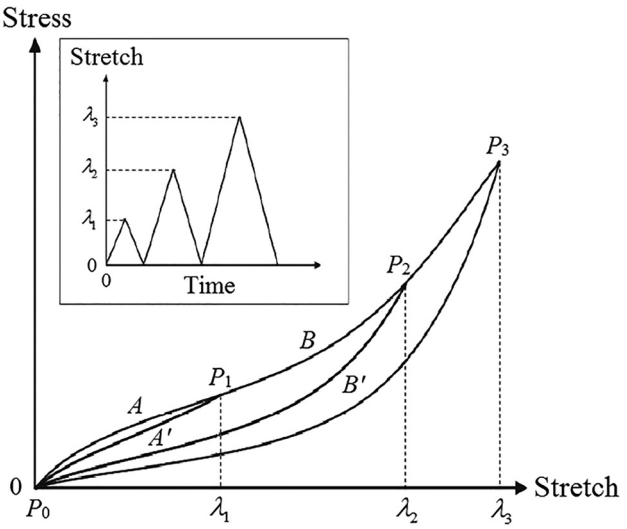

Fig. 2 Stress–stretch relation of idealized Mullins effect

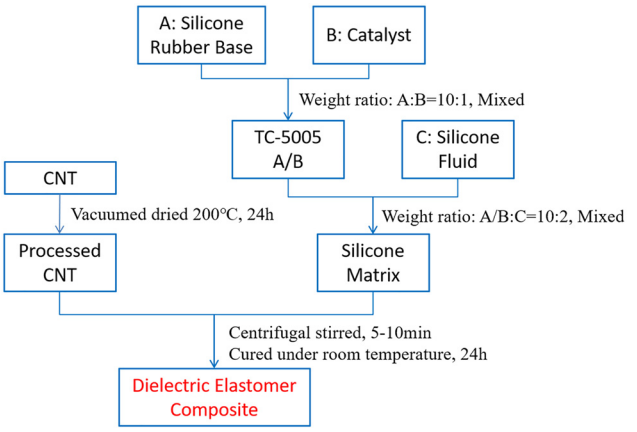

Fig. 3 Preparation process of CNT filled silicon elastomer

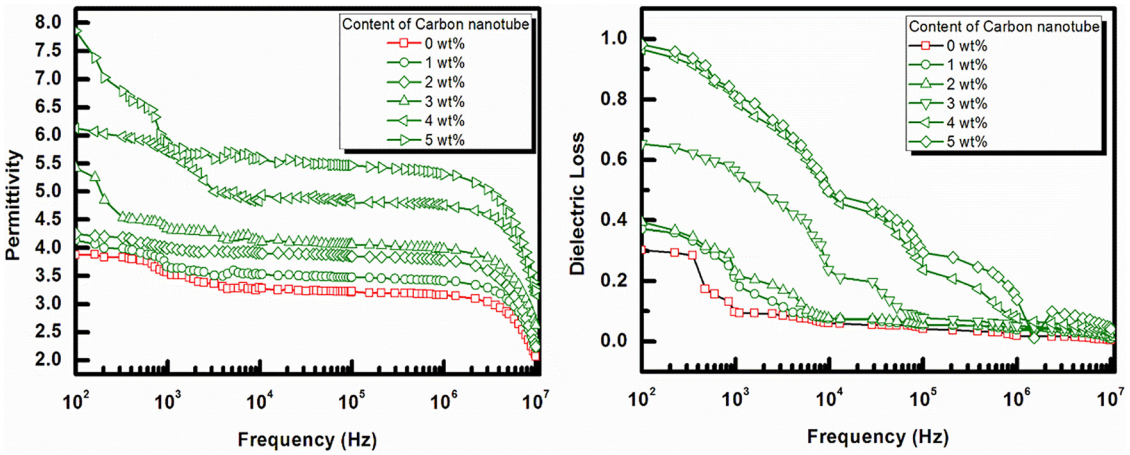

Fig. 4 Relative permittivity and dielectric loss of silicone composite with different CNTs content at varying frequencies [9] (Reprinted with permission from Elsevier © 2015)

3 Modeling of Idealized Mullins Effect

Without interpreting the internal mechanism and merely using the mathematic method, Ogden and Roxburgh [16] developed a phenomenological theory of pseudo-elasticity to characterize Mullins effect. They modified the strain energy function by incorporating an additional variable.

$$\hat{W}(\mathbf{F},\eta) = \eta W_0(\mathbf{F}) + \phi(\eta) \tag{1}$$

where $W_0(\mathbf{F})$ is the strain energy function, η is the damage variable with the maximal value of 1, and $\phi(\eta)$ is the damage function. The damage variable can be active or inactive. When it is inactive ($\eta = 1$), the pseudo-elastic energy recovers elastic, $\hat{W}(\mathbf{F},1) = W_0(\mathbf{F})$. When it is active ($\eta_{\min} \le \eta < 1$), the damage variable changes the mechanical response. The inclusion of damage variable provides a means of changing the strain energy function during the deformation process and consequently changes the character of mechanical response. In general, the mechanical response is never elastic, so $\hat{W}(\mathbf{F},\eta)$ is called pseudo-elastic model.

For uniaxial stretch, the constitutive equation incorporating Mullins effect can be simplified as

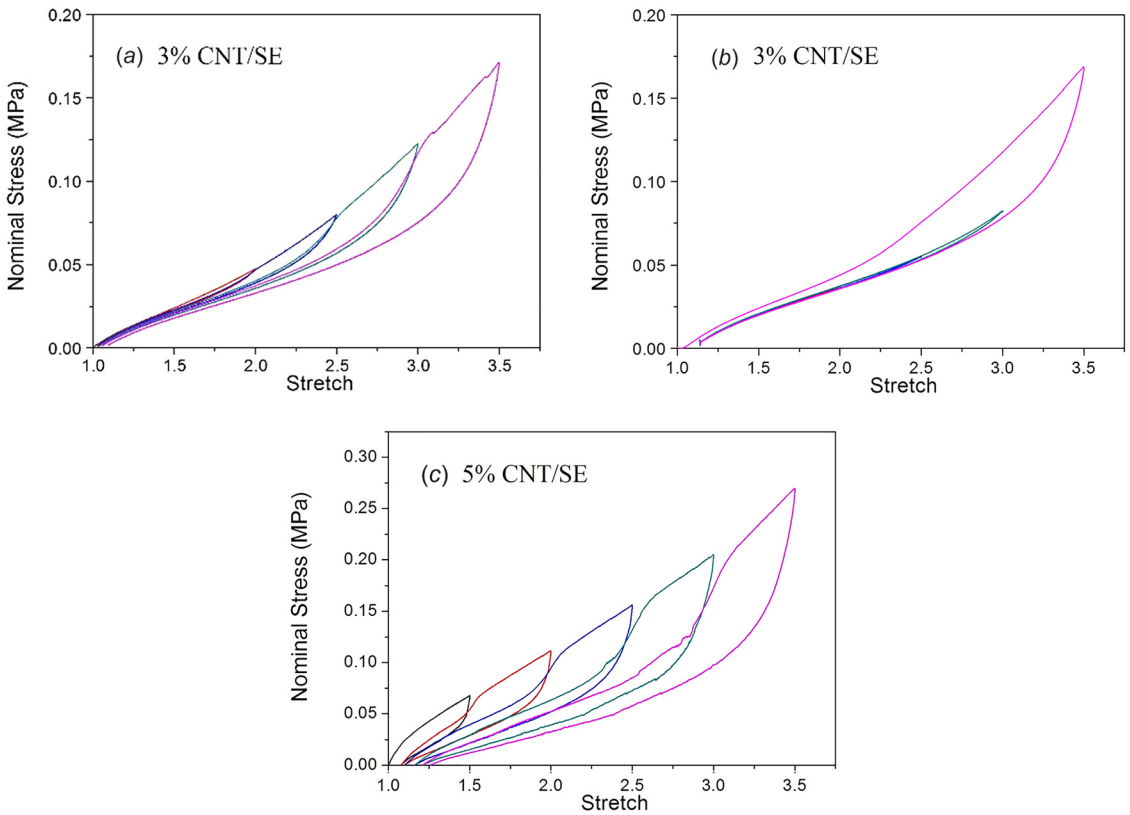

Fig. 5 Step-up (*a*) and step-down (*b*) curves for 3% CNT/SE and step-up curves for 5% CNT/SE

Table 1 Fitting parameters for 5% CNT/SE

Model	Neo-hookean	Mooney–Rivlin		Yeoh		
Parameter	C_{10}	C_{10}	C_{01}	C_{10}	C_{20}	C_{30}
	0.03524	0.0424	−0.01904	0.03193	-3.08801×10^{-6}	2.64232×10^{-5}

$$s = \eta \frac{\partial W_0(\lambda)}{\partial \lambda} \tag{2}$$

The former part is the damage variable, while the latter part is the classical elastic response of rubber material. For Mullins effect, when unloading starts, the damage variable changes from inactive to active. Actually, the damage variable acts as a softening function here. Researchers have established various types of damage function; see for instance Refs. [16–19].

As the 5% CNT/SE shows obvious Mullins effect, we utilize its step-up test data to study in the rest of this paper. The experimental result must be processed as only idealized Mullins effect is focused here, we follow the steps in literatures [23,24]: replace the upper boundary by the pervious fitting curve; remove the reloading curves, and consider they follow the unloading curves; unloading curves are horizontally moved to point (1, 0) to eliminate the residual strain.

To model Mullins effect, a proper strain energy function and damage variable should be given. For an incompressible rubber material, strain energy function can be regarded as a function of the first and second invariant [25,26]:

$$W = \sum_{i,j=0}^{\infty} C_{ij}(I_1 - 3)^i (I_2 - 3)^j \tag{3}$$

where C_{ij} are the material constants, and the term C_{00} is always taken as a null value.

This model is quite complicated; thus, we start from the simplest from until the accuracy meets our need. Neo-hookean model [25,26], Mooney–Rivlin model [27], and Yeoh model [28] are fitted. Fitting results are shown in Table 1 and Fig. 6(*a*). We find Yeoh model with three material parameters

$$W_{\text{Yeoh}} = \sum_{i=0}^{3} C_{i0}({\lambda_1}^2 + {\lambda_2}^2 + {\lambda_3}^2 - 3)^i \tag{4}$$

fits well with our experimental data, and it will be used in the following analysis.

Since the damage variable proposed by Yeom et al. [19] contains an additional nonlinear term which can account for highly nonlinear behavior, we adopt their model in our fitting and analysis. The damage variable is given as

$$\eta = \left[1 - \frac{1}{r}\tanh\left(\frac{W_{\max} - W_0(\lambda)}{mW_{\max}}\right)\right]\left(\frac{W_0(\lambda)}{W_{\max}}\right)^n \tag{5}$$

where r, m, and n are material constants. Fitting results are shown in Table 2 and Fig. 6(*b*). We can see the model fitting basically well with the experiment when the stretch is larger than 1.5. These parameters will be used in the following analysis.

4 Idealized Electromechanical Softening Behavior

Following Suo's theory [29], when undergoing homogenous deformation, the constitutive relation of dielectric elastomer under electromechanical coupling field can be determined by its free energy function W.

$$s_i = \frac{\partial W(\lambda_1, \lambda_2, \lambda_3, \tilde{D})}{\partial \lambda_i} \quad (i = 1, 2, 3) \tag{6a}$$

$$W(\lambda_1, \lambda_2, \lambda_3, \tilde{D}) = W_S(\lambda_1, \lambda_2, \lambda_3) + W_P(\lambda_1, \lambda_2, \lambda_3, \tilde{D}) \tag{6b}$$

where W_S and W_P are the contributions due to stretching and polarizing, respectively, $s_i (i = 1, 2, 3)$ are the nominal stresses, $\lambda_i (i = 1, 2, 3)$ are the stretches in principal directions, and $\tilde{D}$ is the nominal electric displacement. If a free energy function W is given, the state of dielectric elastomer will be determined.

The dielectric elastomer material is considered incompressible, namely

$$\lambda_1 \lambda_2 \lambda_3 = 1 \tag{7}$$

To account for stress softening, we replace the contribution from stretching by pseudo-elastic model, the state equations (6) of incompressible dielectric elastomer become

$$s_i - \frac{s_3}{\lambda_i^2 \lambda_j} = \frac{\partial W_s^{\wedge}(\lambda_1, \lambda_2)}{\partial \lambda_i} + \frac{\partial W_P(\lambda_1, \lambda_2, \tilde{D})}{\partial \lambda_i} \quad (i, j = 1, 2 \text{ and } i \neq j) \tag{8}$$

The dielectric material can polarize under electric field. For dielectric elastomers, the polarization is caused by the rotation of dipoles. When the electric field is low, the polarization is linear and small; when the electric field is sufficient high, all dipoles arrange perfectly along the direction of electric field, the polarization is saturated. Usually, the electric displacement can be expressed as $D = \varepsilon_0 E + P$, where ε_0 is the vacuum permittivity and P the polarization. In our previous work, we gave a formulated relation of electric displacement to account for polarization saturation but ignoring the first term [30]. We modify the expression as

$$D = \varepsilon_0 E + P_s \tanh\left(\frac{\varepsilon - \varepsilon_0}{P_s} E\right) \tag{9}$$

where ε_0 is the vacuum permittivity, ε is the permittivity of DE, and P_s is the saturated polarization. When $(\varepsilon - \varepsilon_0)E/P_s \ll 1$, the relation between E and D recovers linear, $D = \varepsilon E$; when $(\varepsilon - \varepsilon_0)E/P_s \gg 1$, the polarization saturates, $D = \varepsilon_0 E + P_s$.

The contribution from polarizing can be obtained by integrating $\int_0^D E dD$ [29]. However, it is nearly impossible to analytically express E from Eq. (9); therefore, we make the following simplification: the electric displacement is all linear before polarization saturation. Then, we have the corresponding electric energy

$${W_p}^L(\lambda_1, \lambda_2, \tilde{D}) = \frac{\tilde{D}^2}{2\varepsilon} \lambda_1^{-2} \lambda_2^{-2} \quad \text{when } E < E_s \tag{10a}$$

$${W_p}^H(\lambda_1, \lambda_2, \tilde{D}) = \frac{\tilde{D}^2}{2\varepsilon_0} \lambda_1^{-2} \lambda_2^{-2} - \frac{\tilde{D} P_s}{\varepsilon_0} \lambda_1^{-1} \lambda_2^{-1} + \frac{\varepsilon {P_s}^2}{2\varepsilon_0(\varepsilon - \varepsilon_0)} \quad \text{when } E > E_s \tag{10b}$$

where E_s is the electric field when polarization is saturated.

We consider equal-biaxial deformation, namely $\lambda_1 = \lambda_2 = \lambda$, and use the Yeoh model (4) and the damage variable (5), the dimensionless state equations can be obtained

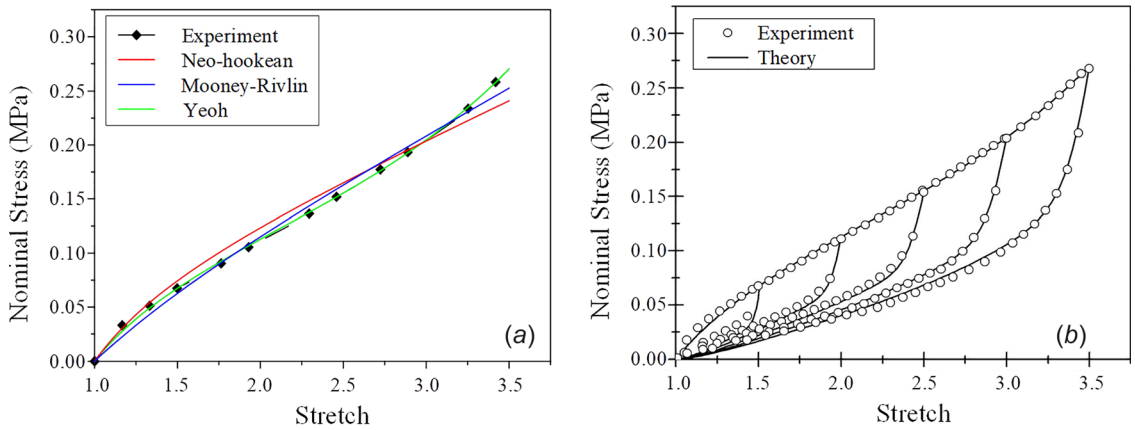

Fig. 6 Fitting results with different models (*a*) and of Mullins effect (*b*)

Table 2 Fitting parameters of Mullins effect

Parameter	r	m	N
Value	2.397974	0.132968	0.29536

$$\frac{s}{C_{10}} = \eta(\lambda)\frac{\partial W_{\text{Yeoh}}(\lambda)}{\partial \lambda} - \left(\frac{\tilde{E}}{\sqrt{C_{10}/\varepsilon}}\right)^2 \lambda^3 \tag{11a}$$

$$\frac{s}{C_{10}} = \eta(\lambda)\frac{\partial W_{\text{Yeoh}}(\lambda)}{\partial \lambda} - \left(\frac{\tilde{E}}{\sqrt{C_{10}/\varepsilon_0}}\right)^2 \lambda^3 - \frac{\tilde{E}}{\sqrt{C_{10}/\varepsilon_0}}\frac{P_s}{\sqrt{C_{10}\varepsilon_0}}\lambda \tag{11b}$$

In the following analysis, we use the fitting parameters of 5% CNT/SE to predict the electromechanical softening behavior. We assume all the equilibrium states and loading processes can be realized, and only describe the theoretical curves of the highly nonlinear softening behavior.

First, we focus on the first case: the electric field is low so that the dielectric is far less than polarization saturation, or the DE material is considered to be an ideal linear dielectric. Figure 7 shows the curves of nominal electric field versus stretch and nominal stress versus stretch under different electromechanical coupling situations. In Fig. 7(*a*), the existing force acts as a dead load prestretch, which improves the voltage-induced deformation. The existing force moves the curve to the right, resulting in a larger stretch with same voltage. Also, the prestretch lowers the threshold of instability. As the force increases, the declining rate of the left local maximum point is faster than the right local minimum point, which will definitely cause the two local extreme points vanish. Therefore, instability is eliminated. In Fig. 7(*b*), with the increasing of voltage, the stress–stretch response changes from monotonous to nonmonotonous, showing an up-down-up shape.

Figure 8 shows the voltage-controlled loading and unloading curves with $s/C_{10} = 0$ and $s/C_{10} = 1$. Due to softening, the unloading lowers the critical snap-through voltage, thus causing some interesting phenomena. If the equilibrium state at the stretch of 2.5 on the loading curve can be obtained, two snap-through processes may exist during reloading, see Fig. 8(*a*), however, the equilibrium state in the descending branch is nearly impossible to obtain. In a voltage-controlled loading and unloading, the process follows the path O-A-B-C-D-E-O; in the subsequent reloading and unloading, the process will follow the path O-F-H-C-D-E-O. The DE material is usually prestretched to improve its voltage-induced deformation or to eliminate electromechanical instability. In the electromechanical coupling loading situation, the existing force acts as a dead load prestretch. In Fig. 8(*b*), the unloading curves will never go back to the starting point, which looks like "residual strain." It is caused by softening; the decreasing modulus enlarges stretch under same force. We can also observe that snap-through instability is eliminated during the reloading process.

Figure 9 shows the force-controlled loading and unloading curves with $\tilde{E}/\sqrt{C_{10}/\varepsilon} = 0.25$ and $\tilde{E}/\sqrt{C_{10}/\varepsilon} = 0.55$. If the applied voltage is low, the curves have the similar trend with the only force-controlled case; compare Figs. 6(*b*) and 9(*a*). If the initial voltage is sufficient high, the electromechanical coupling has a strong impact on the material response, resulting in a highly nonlinear behavior with an N-shaped force-controlled loading

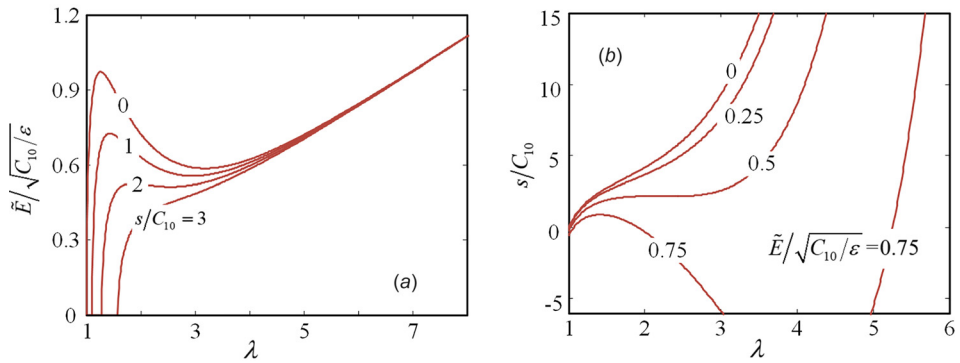

Fig. 7 Nominal electric field—stretch curves with different initial forces (*a*) and nominal stress–stretch curves with different initial voltages (*b*)

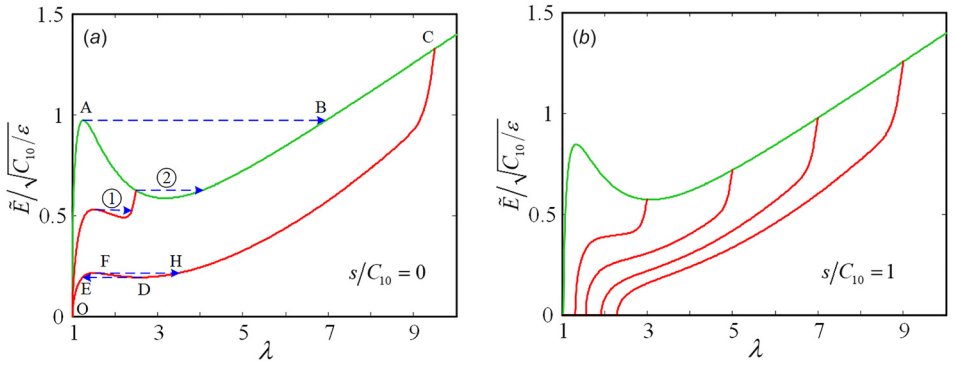

Fig. 8 Idealized voltage-controlled loading and unloading curves with $s/C_{10}=0$ (*a*) and $s/C_{10}=1$ (*b*)

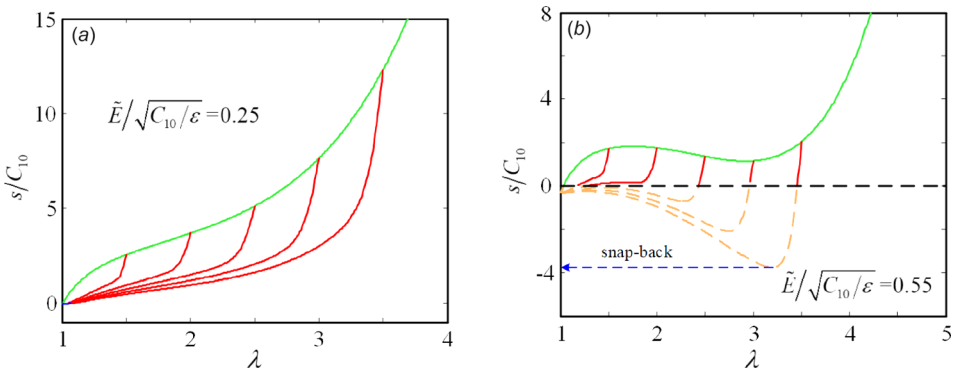

Fig. 9 Idealized force-controlled loading and unloading curves with $\tilde{E}/\sqrt{C_{10}/\varepsilon}=0.25$ and $\tilde{E}/\sqrt{C_{10}/\varepsilon}=0.55$

curve (Fig. 9(*b*)), which is similar as the curves in voltage-controlled cases. As we prescribe that the stretch starts form 1, the existing voltage will cause a negative starting force, and it will definitely have a change from negative to positive. See Fig. 9(*b*), the negative stress (orange dashed lines) exists in an extensive stretch range during unloading. Meanwhile, the reversed increasing force will trigger snap-back at local minimum point.

Then, we consider the second case: the electric field is sufficient high so that the polarization of dielectric elastomer is fully saturated. In our simplification, the dielectric elastomer is linear dielectric before E_s, while the polarization is saturated after E_s; the critical electric field $\tilde{E}_s/\sqrt{C_{10}/\varepsilon_0}=(P_s/\sqrt{C_{10}\varepsilon_0}/(\varepsilon_r-1)\lambda^2)$, where $\varepsilon_r=\varepsilon/\varepsilon_0$ is the relative permittivity. Suitable initial $\tilde{E}/\sqrt{C_{10}/\varepsilon_0}$ and $P_s/\sqrt{C_{10}\varepsilon_0}$ need be determined to meet this condition. From Fig. 4, 5% CNT/SE has a ε_r value of 5 in a wide range of frequency, so $\tilde{E}/\sqrt{C_{10}/\varepsilon}=\sqrt{5}\tilde{E}/\sqrt{C_{10}/\varepsilon_0}$. We plot the nominal electric field versus stretch relations with various $P_s/\sqrt{C_{10}\varepsilon_0}$ in Fig. 10(*a*). For linear model, the relation follows the blue curve, and snap-through from A to B happens under continuous loading. Considering polarization saturation, the curves follow the linear model at the beginning as the electric field is low, then turn to the paths of saturated model (green curves) after reaching E_s. When the saturated polarization is small ($P_s/\sqrt{C_{10}\varepsilon_0}=1$), the DE is easy to saturate under low voltage, and also the critical voltage to trigger snap-through is increased. As $P_s/\sqrt{C_{10}\varepsilon_0}$ increases, snap-through disappears. When $P_s/\sqrt{C_{10}\varepsilon_0}=10$, the snap-through deformation decreases; see in Fig. 10(*a*). Therefore, it can be concluded that the polarization saturation can enhance the stability of electromechanical coupling system of dielectric elastomer. Figure 10(*b*) plots the unloading

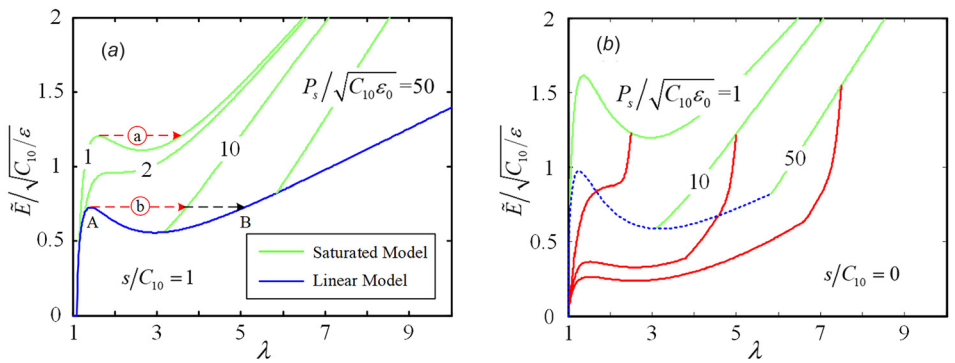

Fig. 10 Nominal electric field—stretch curves (*a*) and idealized voltage-controlled loading and unloading curves (*b*) for saturated model with various $P_s/\sqrt{C_{10}\varepsilon_0}$

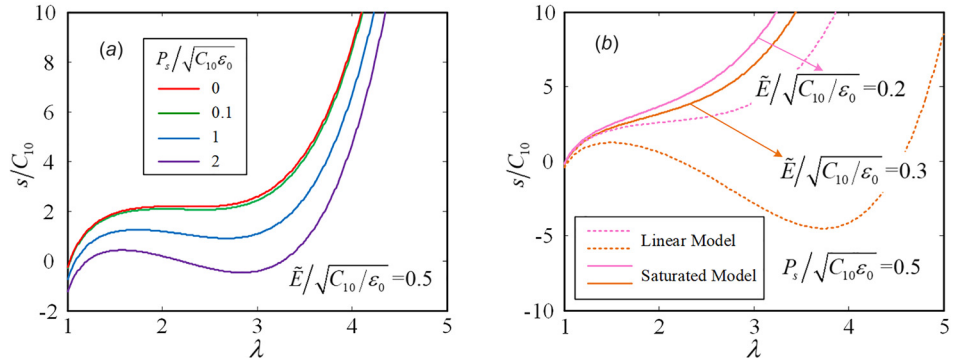

Fig. 11 Nominal stress–stretch curves with various saturated polarizations (*a*) and different initial voltages (*b*)

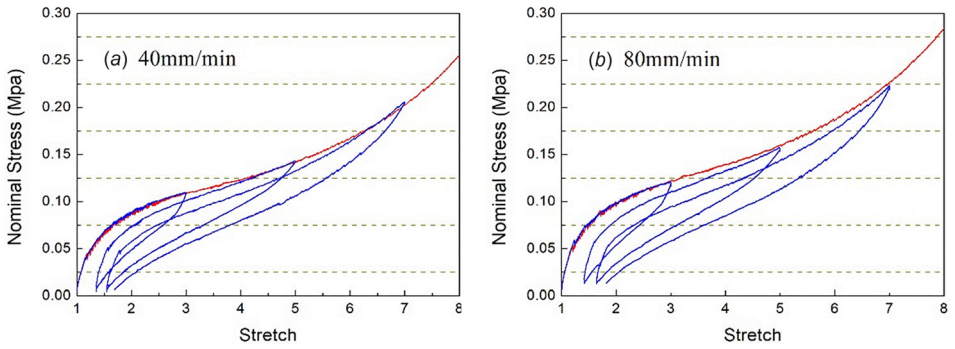

Fig. 12 Tensile curves (red) and step-up curves (blue) for VHB 4910 under different loading rate (*a*) 40 mm/min and (*b*) 80 mm/min

paths (red curves) for saturated model when $s/C_{10} = 0$. From Fig. 8(*a*), reloading at $\lambda = 2.5$ has two snap-through processes. But the one caused by softening disappears ($P_s/\sqrt{C_{10}\varepsilon_0} = 1$). Because polarization saturation affects Maxwell stress, the softening behavior, compared with the red curves in Fig. 8(*a*), also changes when DE undergoing polarization saturation.

Figure 11(*a*) presents the influence of $P_s/\sqrt{C_{10}\varepsilon_0}$ on stress versus stretch relation. We set two groups of values, when $\tilde{E}/\sqrt{C_{10}/\varepsilon_0} = 0.5$, $P_s/\sqrt{C_{10}\varepsilon_0} = 0.1$, $P_s/\sqrt{C_{10}\varepsilon_0} = 1$. and $P_s/\sqrt{C_{10}\varepsilon_0} = 2$; when $P_s/\sqrt{C_{10}\varepsilon_0} = 0.5$, $\tilde{E}/\sqrt{C_{10}/\varepsilon_0} = 0.2$, and $\tilde{E}/\sqrt{C_{10}/\varepsilon_0} = 0.3$ When the saturated polarization P_s is small, the linear term $\varepsilon_0 E$ in Eq. (9) dominates the electric displacement D, the curve is nearly close to the ideal linear case (red and green curves); while with the increasing of P_s, the second nonlinear term takes the main role so that the curves become nonmonotonic (blue and purple curves). Figure 11(*b*) compares the linear model and saturated model. Physically, polarization saturation decreases the Maxwell stress, resulting in a higher stress level under same voltage. Besides, the curves tend to be monotonous, that is to say the polarization saturation can make the electromechanical coupling system of dielectric elastomer more stable. The unloading behaviors are expected to be similar as the cases in Fig. 9, which will not be repeated here.

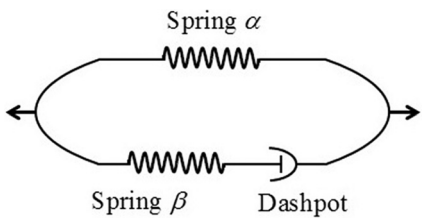

Fig. 13 Viscoelastic model consists of springs and dashpot

5 Viscoelasticity and Electromechanical Testing

In the previous analysis, the mechanical response of material is considered fully elastic. However, viscoelasticity is a typical trait of dielectric elastomer. In this section, we work on VHB 4910 material, since the commercial material has good performance stability and strong viscoelasticity. Also, the wide using of the VHB material in real applications makes the experiments significant. Same step-up test as in Sec. 2 was conducted on VHB 4910. We set two loading rates: 40 mm/min and 80 mm/min, and step strain 100%. It can be seen from the testing curves (Fig. 12) that stress softening and residual strain appear obviously. Viscoelasticity lowers the stress level under low loading rate. Besides, it is worth noting that the tensile curve forms the upper boundary of the step-up curves, which is very close to the idealized Mullins effect assumption.

To account for rate-dependent deformation, the viscoelastic model, consisting of two springs and one dashpot [31,32] (as shown in Fig. 13), is introduced into the theory. According to multiplication rule, the stretch in spring α is the multiplication of the stretches of spring β and dashpot, $\lambda_1^A = \lambda_1^B \xi_1$ and $\lambda_2^A = \lambda_2^B \xi_2$.

In order to incorporate softening, we replace the energy of spring α by pseudo-elastic energy model. The total energy of the dielectric elastomer is the sum of the contribution of the two springs

Table 3 Fitting parameters of Yeoh model and damage variables

Parameter	C_{10}	C_{20}	C_{30}	r	m	n
Value	0.01996	-1.43718×10^{-4}	1.17624×10^{-6}	3.026	0.453	0.051

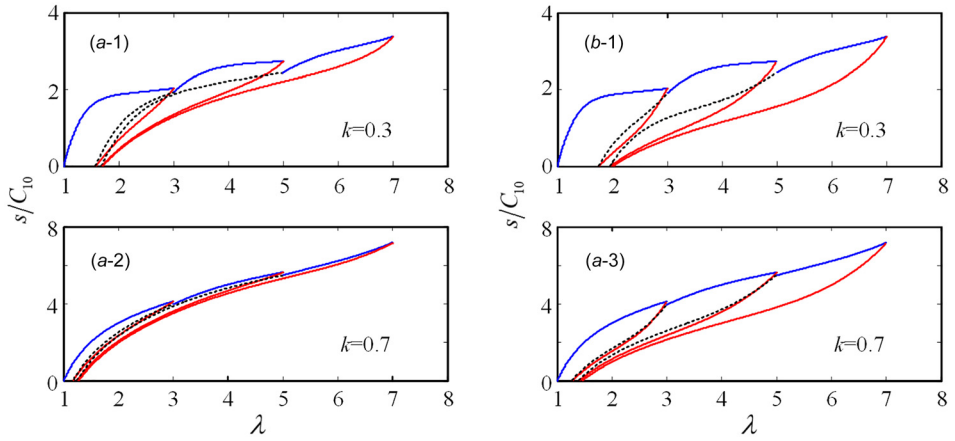

Fig. 14 Nominal stress–stretch curves with $\tau_v = 100$ s and different k using viscoelastic model (*a*) and pseudo-elastic–viscoelastic model (*b*)

$$W_S(\lambda_1, \lambda_2, \xi_1, \xi_2, \eta) = k\hat{W}_A(\lambda_1, \lambda_2, \eta) + (1-k)W_B(\lambda_1\xi_1^{-1}, \lambda_1\xi_2^{-1}) \quad (12)$$

where $0 \le k \le 1$ is the constant which determines the viscoelasticity.

The stretch rate in the dashpot can be described as

$$\frac{d\xi_i}{\xi_i dt} = \frac{1}{3\eta}\left(\lambda_i \frac{\partial W_B}{\partial \lambda_i} - \lambda_j \frac{\partial W_B/2}{\partial \lambda_j}\right) \quad (i, j = 1, 2 \text{ and } i \ne j) \quad (13)$$

where η is the viscosity of the dashpot.

We first find out a set of available parameters by fitting the experimental curves using the idealized model. In our experiment, the curve patterns have same trend although the loading rate varies. Table 3 gives a set of acceptable fitting parameters for loading rate 40 mm/min.

In the viscoelastic model, the above Yeoh parameters are used for the two springs, and we simulate different viscoelastic behavior by adjusting k. We introduce relaxation time $\tau_v = \eta/C_{10}$ to make Eq. (13) dimensionless. Figure 14 plots the theoretical results using viscoelastic model (a) and pseudo-elastic-viscoelastic model (b), respectively. The blue curves represent

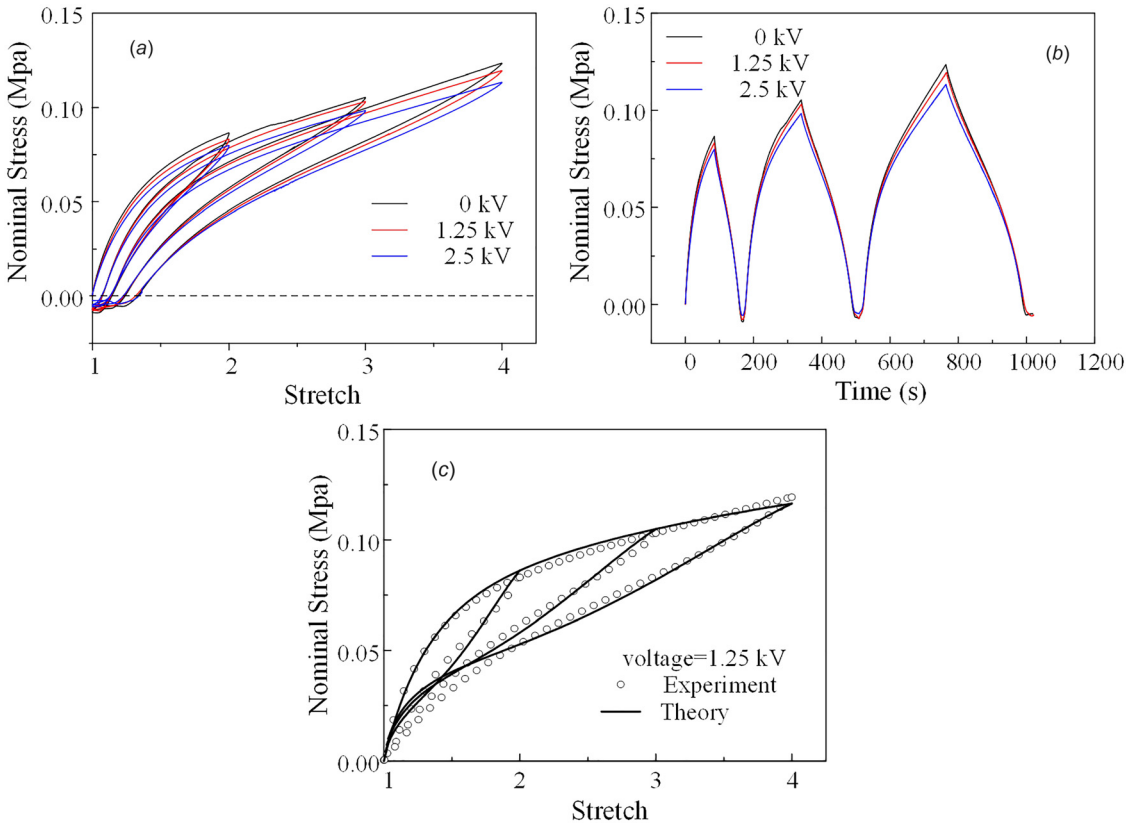

Fig. 15 Force–strain curves (*a*) and force–time curves (*b*) with different initial voltages and the comparison of fitting and experimental curves at 1.25 kV (*c*)

loading paths; the red curves represent unloading paths; while the black dotted curves represent the reloading paths before reaching the former unloading points. Compared with the idealized model, viscoelastic model accounts for residual strain, and separates the unloading and reloading curves. We can find that k affects the material response greatly. Larger k corresponds to higher stress level, smaller residual strain and closer unloading and reloading curves. It is easy to understand from the theoretical model: spring α determines softening and elastic deformation; spring β together with dashpot determine viscous deformation, while k determines the proportion of the two parts in the model. A larger k means the DE is closer to an elastic material, which has lower relaxation, smaller hysteresis and more idealized Mullins effect. Further, comparing the two models, the stress softens obviously in (b-1) and (b-2), due to the pseudo-elastic model.

Then, we carried out some simple experiments to explore the electromechanical situation. Pure shear VHB 4910 specimens with effect dimensions 100 mm × 10 mm × 1 mm were tested. The electromechanical loading was also conducted on Zwick/Roell Z010 universal testing machine. The electric loads were applied on the specimens through a function signal generator and voltage amplifier.

We conducted a force-controlled test with different initial voltages. We set the loading rate 10 mm/min, and the step strain is 100%. Different initial voltages, 0 kV, 1.25 kV, and 2.5 kV, were applied throughout the experiment. The recorded force–strain curves are shown in Fig. 15(*a*). As the theoretical predictions only consider the idealized situation, we remove the reloading curves, and compare the remaining curves with Fig. 9(*a*). The initial force starts from negative, and the stress softens after every cycle. Comparing the curves with different voltages, large initial voltage corresponds to lower stress level, which is consistent with our experience. This fact can also be obvious found in the peak area in force–time curves (Fig. 15(*b*)). The parameters used in Fig. 9(*a*) are from 5% CNT/SE, not VHB 4910, so we further fit the experiment results of 1.25 kV with linear model in Fig. 15(*c*).

Different from a mechanical test, it is hard to control the loading, unloading, and reloading in a constant strain rate by voltage. We fixed the pure-sheared VHB 4910 specimens at 300% strain, and then apply an AC voltage with amplitude 3 kV and frequency 0.05 Hz. We expected to read the force change during the application of AC voltage. When the AC voltage is on, the active area expands; the force will reach a local minimum at the peak of AC voltage. If the material softens after every cycle, the force to maintain the fixed strain will drop. But in the practical experiment, although we recorded the force minimum and the force drop, the strong viscoelasticity-induced stress relaxation exists; it is hard to tell to what extent the softening contributes to the phenomenon. But we still believe the softening happens under the repeated voltage. Thus, it is a challenge to investigate the softening behavior under voltage-controlled process. We hope to discuss more about this area in the future.

6 Conclusions

In this paper, we investigated the electromechanical softening behavior of CNT filled silicon elastomer and VHB 4910. We prepared the carbon nanotube filled silicon elastomer and characterized its softening behavior by stepwise cyclic tensile test. Based on the pseudo-elastic theory, we modeled the Mullins effect, and the model fits well with the stepwise cyclic tensile test. Then we investigated the idealized softening behavior under electromechanical coupling field by combining the thermodynamics of DE and pseudo-elastic theory. Two cases are considered: linear dielectric and saturated dielectric. For linear dielectric with an initial force, because of softening, "residual strain" will appear after every voltage-controlled cycle, and instability may be eliminated in reloading. For saturated dielectric, we assume the dielectric is all linear before polarization saturation. After saturation, the material response changes a lot, which also affects the following softening behavior. At last, viscoelasticity was further incorporated to account for rate-dependent softening deformation, and we also carried out some simple electromechanical experiments on 4910 to explore its softening behavior.

In our paper, we provide a broadly applicable method to study softening behavior under electromechanical coupling field, the research object can be extended into a class of material—the soft deformable dielectrics, and the conclusions are expected to be similar. However, due to the limit of conditions, how to fully demonstrate these results is still a challenge. We hope to discuss these matters in future.

Funding Data

- The National Natural Science Foundation of China: Grant Nos. 11672086, 11772109, and 11632005.

References

[1] Pelrine, R., Kornbluh, R., Pei, Q. B., and Joseph, J., 2000, "High-Speed Electrically Actuated Elastomers With Strain Greater Than 100%," Science, **287**(5454), pp. 836–839.

[2] Carpi, F., Bauer, S., and DeRossi, D., 2010, "Stretching Dielectric Elastomer Performance," Science, **330**(6012), pp. 1759–1761.

[3] Brochu, P., and Pei, Q. B., 2010, "Advances in Dielectric Elastomers for Actuators and Artificial Muscles," Macromol. Rapid Commun., **31**(1), pp. 10–36.

[4] Bar-Cohen, Y., 2000, "Electroactive Polymers as Artificial Muscles Capabilities, Potentials and Challenges," *Handbook on Biomimetics*, Y. Osada, ed., NTS Inc., Bakersfield, CA, pp. 1–13.

[5] Bar-Cohen, Y., 2006, "Biologically Inspired Technology Using Electroactive Polymers (EAP)," Proc. SPIE, **6168**, p. 616803.

[6] Liu, Y. J., Liu, L. W., Zhang, Z., Jiao, Y., Sun, S. H., and Leng, J. S., 2010, "Analysis and Manufacture of an Energy Harvester Based on a Mooney-Rivlin-Type Dielectric Elastomer," Europhys. Lett., **90**(3), p. 36004.

[7] Lv, X. F., Liu, L. W., Liu, Y. J., and Leng, J. S., 2015, "Dielectric Elastomer Energy Harvesting: Maximal Converted Energy, Viscoelastic Dissipation and a Wave Power Generator," Smart Mater. Struct., **24**(11), p. 115036.

[8] Liu, L. W., Liu, Y. J., Zhang, Z., Li, B., and Leng, J. S., 2010, "Electromechanical Stability of Electro-Active Silicone Filled With High Permittivity Particles Undergoing Large Deformation," Smart Mater. Struct., **19**(11), p. 115025.

[9] Liu, L. W., Zhang, Z., Li, J. R., Li, T. F., Liu, Y. J., and Leng, J. S., 2015, "Stability of Dielectric Elastomer/Carbon Nanotube Composites Coupling Electrostriction and Polarization," Compos. Part B: Eng., **78**, pp. 35–41.

[10] Bueche, F., 1960, "Molecular Basis for the Mullins Effect," J. Appl. Polym. Sci., **4**(10), pp. 107–114.

[11] Bueche, F., 1961, "Mullins Effect and Rubber–Filler Interaction," J. Appl. Polym. Sci., **5**(15), pp. 271–281.

[12] Mullins, L., 1948, "Effect of Stretching on the Properties of Rubber," Rubber Chem. Technol., **21**(2), pp. 281–300.

[13] Mullins, L., 1969, "Softening of Rubber by Deformation," Rubber Chem. Technol., **42**(1), pp. 339–362.

[14] Lu, T. Q., Wang, J. K., Yang, R. S., and Wang, T. J., 2017, "A Constitutive Model for Soft Materials Incorporating Viscoelasticity and Mullins Effect," ASME J. Appl. Mech., **84**(2), p. 021010.

[15] Mullins, L., and Tobin, N. R., 1957, "Theoretical Model for the Elastic Behavior of Filler-Reinforced Vulcanized Rubbers," Rubber Chem. Technol., **30**(2), pp. 555–571.

[16] Ogden, R. W., and Roxburgh, D. G., 1999, "A Pseudo-Elastic Model for the Mullins Effect in Filled Rubber," Proc. R. Soc. London A, **455**(1988), pp. 2861–2877.

[17] Dorfmann, A., and Ogden, R. W., 2003, "A Pseudo-Elastic Model for Loading, Partial Unloading and Reloading of Particle-Reinforced Rubber," Int. J. Solids Struct., **40**(11), pp. 2699–2714.

[18] Dorfmann, A., and Ogden, R. W., 2004, "A Constitutive Model for the Mullins Effect With Residual Strain in Particle Reinforced Rubber," Int. J. Solids Struct., **41**(7), pp. 1855–1878.

[19] Yeom, K. S., Jeong, S., Huh, H., and Park, J., 2013, "New Pseudo-Elastic Model for Polymer-Bonded Explosive Simulants Considering the Mullins Effect," J. Compos. Mater., **47**(27), pp. 3401–3412.

[20] Rickaby, S. R., and Scott, N. H., 2013, "A Model for the Mullins Effect During Multicyclic Equibiaxial Loading," Acta Mech., **224**(9), pp. 1887–1900.

[21] Rickaby, S. R., and Scott, N. H., 2013, "Cyclic Stress-Softening Model for the Mullins Effect in Compression," Int. J. Nonlinear Mech., **49**, pp. 152–158.

[22] Rickaby, S. R., and Scott, N. H., 2013, "A Cyclic Stress Softening Model for the Mullins Effect," Int. J. Solids Struct., **50**(1), pp. 111–120.

[23] Chagnon, G., Verron, E., Gorne, T. L., Marckmann, G., and Charrier, P., 2004, "On the Relevance of Continuum Damage Mechanics as Applied to the Mullins Effect in Elastomers," J. Mech. Phys. Solids, **52**(7), pp. 1627–1650.

[24] Loo, M. S., Andriyana, A., Lee, S. L., and Tan, N. H., 2014, "A Continuum Mechanical Modelling of Mullins Effect in Swollen Elastomers," Mater. Res. Innov., **18**(Suppl. 6), pp. 56–60.
[25] Rivlin, R. S., 1948, "Large Elastic Deformations of Isotropic Materials. II, Some Uniqueness Theorems for Pure Homogeneous Deformations," Philos. Trans. Roy. Soc. A, **240**(822), pp. 419–508.
[26] Rivlin, R. S., 1951, "Large Elastic Deformations of Isotropic Materials. VII, Experiments on the Deformation of Rubber," Philos. Trans. Roy. Soc. A, **243**(865), pp. 251–288.
[27] Mooney, M., 1940, "A Theory of Large Elastic Deformation," J. Appl. Phys., **11**(9), pp. 582–592.
[28] Yeoh, O. H., 1990, "Characterization of Elastic Properties of Carbon Black-Filled Rubber Vulcanizates," Rubber. Chem. Technol., **63**(5), pp. 792–805.
[29] Suo, Z. G., 2010, "Theory of Dielectric Elastomers," Acta Mech. Solida Sin., **23**(6), pp. 549–578.
[30] Liu, L. W., Liu, Y. J., Luo, X. J., Li, B., and Leng, J. S., 2012, "Electromechanical Instability and Snap-Through Instability of Dielectric Elastomers Undergoing Polarization Saturation," Mech. Mater., **55**, pp. 60–72.
[31] Hong, W., 2011, "Modeling Viscoelastic Dielectrics," J. Mech. Phys. Solids., **59**(3), pp. 637–650.
[32] Foo, C. C., Cai, S. Q., Koh, S. J. A., Bauer, S., and Suo, Z. G., 2012, "Model of Dissipative Dielectric Elastomers," J. Appl. Phys., **111**(3), p. 034102.